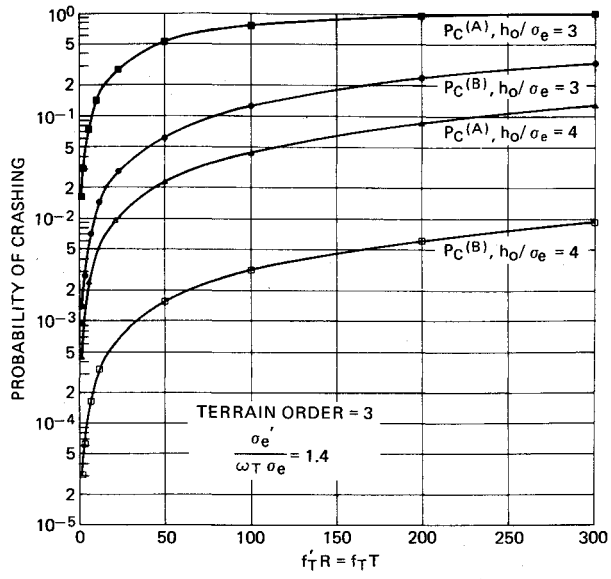

Fig. 4 Comparison of crash probability vs number of terrain cycles.

Thus, for large n

$$P_{NC}^{(B)} \approx \exp(-\nu) = \exp(-\lambda_B T) \tag{17}$$

where

$$\lambda_B = (\omega_T/2\pi)[\tfrac{1}{2} - \mathrm{erf}(h_o/\sigma_e)] \tag{18}$$

Strictly speaking, λ_B as derived, is the average frequency of event B where $B = \{$one or more crashes during an independent subinterval of length $\tau_T\}$. We can write Eq. (8) as

$$\lambda = (\omega_T/2\pi) f(\theta) \exp(-h_o^2/2\sigma_e^2) \tag{19}$$

where $f(\theta) = \sigma_{e'}/(\omega_T \sigma_e)$ (see Table 1). Comparing Eqs. (18) and (19) we note that λ_B is independent of θ. Using τ_e instead of τ_T in deriving Eq. (18) would change this.

Figure 3 shows how the probability of crashing computed from expressions (6) and (14) for different h_o/σ_e ratios compare under the same set of conditions. It is evident that the missile would have to fly higher in order to have $P_C^{(A)}$ equal to $P_C^{(B)}$. Similar information is conveyed in an alternative form in Fig. 4 where $P_C^{(A)}$ and $P_C^{(B)}$ are plotted vs the number of terrain cycles in a particular mission. It will be noted that the value of $P_C^{(B)}$ would increase and be closer to $P_C^{(A)}$ under similar conditions if n were set equal to T/τ_e instead of T/τ_T, since, as previously discussed, $\tau_e < \tau_T$ in most practical cases.

References

[1] McHugh, G. C., Stoner, E. E., and Madonna, M. A., "Terrain Avoidance Maneuver Requirements Using a Radar Altimeter," Newsletter SCM-G&C-001, Sept. 6, 1972, McDonnell-Douglas, St. Louis, Mo.

[2] Weinstein, J. W., "Terrain Following Studies," TN GS-73-1, March 21, 1973, E Systems Inc.,

[3] Whittle, P., "On Stationary Processes in the Plane," *Biometrika*, Vol. 41, 1954, pp. 434–449.

[4] Webber, W. F., "On the Statistical Analysis of Random Surfaces," Ph.D. thesis, 1971, Southern Methodist University, Dallas, Texas.

[5] Newton, G. C., Gould, L. A., and Kaiser, J. F., *Analytical Design of Linear Feedback Controls*, Wiley, New York, 1957, Appendix E.

[6] Cunningham, E. P., "The Probability of Clobber for a Terrain-Following Missile," Internal Memo MCS-0-307, March 1, 1973, Applied Physics Lab., Silver Spring, Md.

[7] Papoulis, A., *Probability, Random Variables and Stochastic Processes*, McGraw-Hill, New York, 1965, Chap. 14.

[8] Beckman, P., *Probability in Communication Engineering*, Harcourt, Brace and World, New York, 1967, Chap. 6.

Particulate Infrared Radiation in Aluminized Solid-Fuel Rocket Plumes

BRUCE W. WORSTER*
Aerodyne Research, Inc., Burlington, Mass.

Introduction

THE far-field infrared emission of solid-propellant rocket exhaust at vacuum-expansion altitudes is of current interest, since such radiation may be an important factor in the detection of these vehicles. Those solid fuels which contain a significant amount of metallic aluminum release most of the metal into the exhaust in the form of oxide (Al_2O_3) particles, whose radius is on the order of microns.[1] These particles have temperatures on the order of the exit-plane gas temperature, and radiate significant amounts of thermal energy.

The formation mechanism of these particles has been treated,[2] as well as their role in engine impulse.[3] Effects of thermal radiation from the optically thick, near-field plume (close to the nozzle), impinging on the vehicle, have been studied.[4] Also, two-phase flow treatments of the motion of these particles in the exhaust have been performed.[5] Most recently, some effort has been made to predict the contribution of particulates to the far-field plume infrared signature of typical vehicles, based on various assumptions about the optical and thermal properties of the particles.[6] This present Note outlines a treatment of the general case of the radiant emission by particulate plumes at IR wavelengths. The parametric results of these computations are in a form applicable to the analysis of field data for the contribution of alumina particles to the total infrared emission of the plume, and for the optical and thermal properties of the particles themselves.

Analysis

The mean-mass particle radius lies in the range 4 to 8 μm for rockets with throat diameters above 5 in.[1] The particle size is of importance because, as predicted by the well-established Mie theory[7,8] emision at a given wavelength, λ, is not inhibited by geometric considerations only when $2\pi r/\lambda \gtrsim 1$, where r is the particle radius. For the infrared wavelengths of interest and the particle-size distributions encountered empirically, the inequality is satisfied.

The specific heat of pure aluminum oxide shows a temperature dependence.[9] The numerical calculations in this work were made assuming the Al_2O_3 in exhausts has the same temperature dependence as the pure substance. Also included in the calculations is the heat of fusion, ΔH_m, released at 2315°K, the melting temperature of Al_2O_3.

In the past, lab measurements of the emissivity of pure alumina in the shorter-wavelength infrared yielded values over the range of 10^{-4} to 10^{-2}. This is in contrast to the emissivities measured in aluminized rocket exhausts,[4] which are typically found to be much larger. Possibly because of polycrystalline or amorphous structure, impurities, and absorption bands at longer IR wavelengths, the exhaust particles exhibit average emissivities on the order of 0.25. Recently made lab measurements of the thermal properties of bulk alumina particles are more consistent with the higher emissivities of the exhaust measurements.[10]

It is important to note that the average emissivity, $\bar{\varepsilon}$, may differ from the spectral emissivity, ε_λ, at a given wavelength, λ. The spectral radiant energy emitted by a given mass of Al_2O_3

Received June 1, 1973; revision received December 6, 1973. This work was sponsored by the Defense Advanced Research Projects Agency under Contract DAA1101-71-C-1291, monitored by the U.S. Army Missile Command.

Index categories: Radiation and Radiative Heat Transfer; Thermal Modeling and Experimental Thermal Simulation.

* Senior Research Scientist.

particles at a given wavelength, λ, during cooling, will depend only on the ratio $\varepsilon_\lambda/\bar{\varepsilon}$, and on the initial temperature.

In this work, the particle plume was taken to be optically thin. For the regions of interest, far downstream from the vehicle, this fact is easily verified.

The spectral energy emitted, per unit surface area, as a particle of spectral emissivity ε_λ cools over a time interval, t_1 to t_2 (and absolute temperature interval T_1 to T_2), is

$$U_\lambda = \int_{t_1}^{t_2} \varepsilon_\lambda R_\lambda{}^0 \, dt = \int_{T_1}^{T_2} \varepsilon_\lambda R_\lambda{}^0 \frac{dt}{dT} dT \tag{1}$$

where $R_\lambda{}^0$ is the Planck black-body function.

By assuming that the surface of the radiating particle can be characterized by a mean emissivity, $\bar{\varepsilon}$ (averaged over any spectral and temperature dependence), the cooling rate of a spherical particle of absolute temperature, T, may be expressed as

$$\frac{dT}{dt} = \frac{-3\bar{\varepsilon}\sigma(T^4 - T_e^4)}{C_p(T)\, r\rho} \tag{2}$$

Here, C_p is the specific heat, ρ is the material density, σ is the Stefan-Boltzmann constant, and T_e is the environment radiation temperature.

By inverting Eq. (2) to obtain dt/dT, the spectral energy, U_λ, emitted per unit mass of particles in cooling from temperature T_1 to T_2, is obtained

$$U_\lambda = -\frac{\varepsilon_\lambda}{\bar{\varepsilon}} \frac{hc^2}{2\sigma\lambda^5} \int_{T_1}^{T_2} \frac{C_p(T)}{[\exp(hc/\lambda kT) - 1](T^4 - T_e^4)} dT \tag{3}$$

where k is Boltzmann's constant, h, Planck's constant, and c, the velocity of light. An interesting feature of Eq. (3) is the fact that the particle radius does not appear, having canceled out in the product of dt/dT and $R_\lambda{}^0$.

Values of Eq. (3) are plotted in Fig. 1, with $T_e = 190°\text{K}$ and $T_2 \gtrsim T_e$, though the particular value of T_e is unimportant for the wavelengths involved; U_λ is insensitive to T_e over a range $230°\text{K} \leqq T_e \leqq 0°\text{K}$ for $\lambda \leqq 13\mu\text{m}$. Here, initial particle temperature, T_1, is treated as a variable, $\varepsilon_\lambda/\bar{\varepsilon}$ is taken as unity, and the temperature dependence of the energy emitted at three different wavelengths (corresponding to regions of atmospheric transparency) is shown. The step increase at $T_2 = 2315°\text{K}$ is due to the heat of fusion released when particles that start as liquid above this temperature solidify. In practice, liquid particles are not expected because they cool below the melting point by convection while still in the near field.

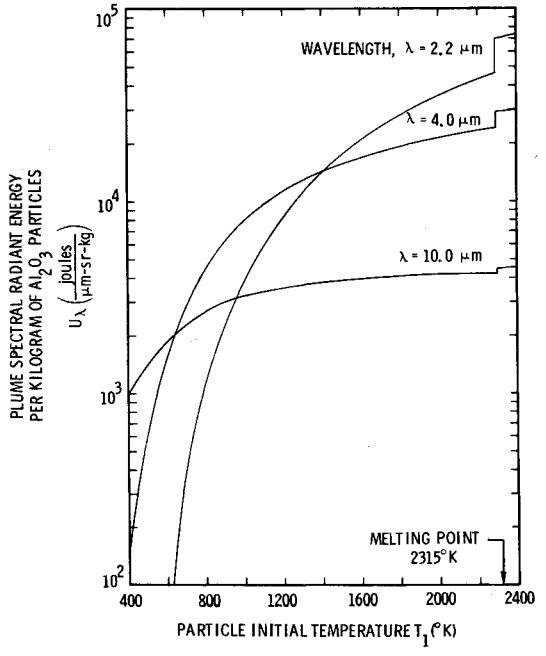

Fig. 1a Dependence of Al_2O_3 particle IR emission on initial particle temperature, T_1, for various IR wavelengths. Here, $\varepsilon_\lambda/\bar{\varepsilon}$ is taken as unity.

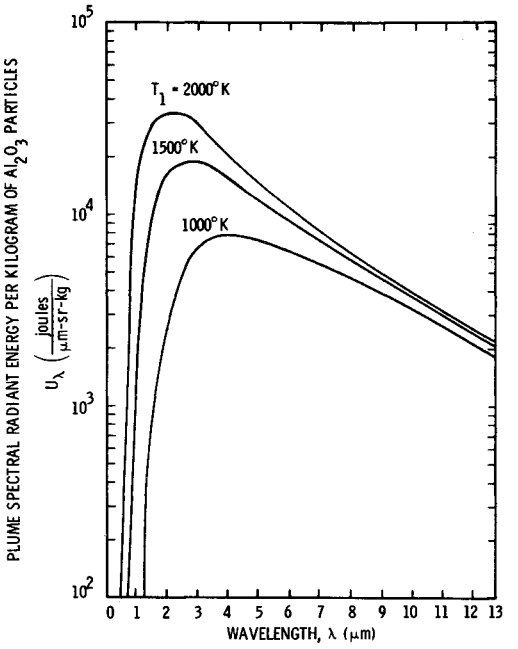

Fig. 1b Dependence of Al_2O_3 particle IR emission on wavelength for various particle initial temperatures, T_1. Here, $\varepsilon_\lambda/\bar{\varepsilon}$ is taken as unity.

The spectral dependence of the energy released during cooling is shown in Fig. 1b for various values of particle initial temperature, T_1. It is seen in Figs. 1a and 1b that the spectral radiant energy becomes increasingly insensitive to particle initial temperature for $\lambda \gtrsim 8$ μm, as long as T_1 is above ~800°K. This is due to the short times that the particles spend at $T \gtrsim 800°\text{K}$; they do not have sufficient time to radiate much energy at the longer wavelengths before cooling to lower temperatures. With decreasing wavelengths, however, U_λ depends increasingly on T_1.

The spectral radiant intensity, J_λ, of a given plume with Al_2O_3 mass-flux $\dot{M}$ is given by $J_\lambda = U_\lambda \dot{M}$. For the units used in Figs. 1a and 1b, $\dot{M}$ is expressed in kg/sec.

Differences between ε_λ and $\bar{\varepsilon}$ at a given wavelength will alter the values plotted in Figs. 1a and 1b. From lab measurements,[10] ε_λ is expected to vary with λ. This variation can be found by analysis of field measurements of the spectral radiant intensity of particle plumes at different wavelengths, and hence, will provide a measure of $\varepsilon_\lambda/\bar{\varepsilon}$. Some variation of sample emittance with temperature in pure alumina has also been observed in lab measurements,[10] but it is not so large as the variations with wavelength. At any rate, this computation of spectral radiant intensity for data analysis purposes must assume, a priori, that ε_λ is averaged over any temperature dependence.

Two-phase flow calculations indicate that conductive cooling becomes insignificant (at vacuum-expansion altitudes) on the order of tens of meters behind the rocket.[5] Furthermore, the solid particles do not cool by sublimation, since this process is an important factor in cooling only above ~2200°K. Hence, the radiative energy-loss process, treated in this section, is the dominant cooling process of the far-field particulate plume.

Field measurements of spectral energy can be and are made without spatial resolution of the plume. It is important, however, to include the entire hot plume within the field-of-view of the instrument in order to compare this radiant intensity model with this data. Here, "hot" refers to temperatures sufficiently high for the particles to radiate significant amounts of energy at the wavelengths of interest. As may be inferred from Fig. 1a, "hot" means, for example, temperatures $\gtrsim 350°\text{K}$ for 10-μm radiation, $\gtrsim 600°\text{K}$ for 4-μm radiation, and $\gtrsim 800°\text{K}$ for 2.2-μm radiation.

From Eq. (2), the time required to cool from a temperature T_1 at time $t = 0$ to a temperature T_2 at time t, is

$$t = -\frac{r\rho}{3\bar{\varepsilon}\sigma}\int_{T_1}^{T_2}\frac{C_p(T)dT}{(T^4 - T_e^4)} \tag{4}$$

Thus, cooling time is seen to be proportional to particle radius and inversely proportional at mean emissivity. For $\bar{\varepsilon} = 0.25$ and particle radii 5 μm, cooling times are $\sim$2 sec for 10-μm radiation. With particle exhaust velocities of 1500 to 2500 m/sec, the radiating plume will be 6 to 10 km long, with the brightest parts within 0.6 to 1.0 km of the rocket nozzle. Particles do not spend much time at the higher temperatures, but cool relatively quickly to lower temperatures. Thus, the total cooling time is very insensitive to particle initial temperature. The most important factors in cooling time are mean emissivity, $\bar{\varepsilon}$, and particle radius, r. This cooling time for the plume observed in field measurements can be analyzed to yield mean particle emissivity, $\bar{\varepsilon}$. This result, combined with a measure of $\varepsilon_\lambda/\bar{\varepsilon}$ as previously discussed, yields ε_λ.

The purpose of this work is to provide a basis for rocket-plume infrared data analysis. Once such measurements determine the emissivity of the rocket exhaust particles, more accurate predictions of particle plume radiant emission profiles can be made.

References

[1] Radke, H. H., Delaney, L. J., and Smith, P., "Exhaust Particle Size Data from Small and Large Solid Rocket Motors," TOR-1001(S2951-18)-3, July 1967, Aerospace Corp., San Bernardino Operations Div., San Bernardino, Calif.

[2] Jenkins, R. M. and Hoglund, R. F., "A Uniform Theory of Particle Growth in Rocket Chambers and Nozzles," AIAA Paper 69-541, U.S. Air Force Academy, Colo., 1969.

[3] Hoglund, R. F., "Recent Advances in Gas-Particle Nozzle Flows," *ARS Journal*, Vol. 32, No. 5, May 1962, pp. 662–671.

[4] Morizumi, S. J. and Carpenter, H. J., "Thermal Radiation from the Exhaust Plume of an Aluminized Composite Propellant Rocket," *Journal of Spacecraft and Rockets*, Vol. 1, No. 5, Sept.–Oct. 1964, pp. 501–507.

[5] Hoffman, R. J., English, W. D., Oeding, R. G., and Weber, W. T., "Plume Contamination Effects Prediction, The Contam Code Computer Program," AFRPL-TR-71-109, Dec. 1971, Air Force Rocket Propulsion Lab., Edwards Air Force Base, Calif.

[6] Cherry, S. S., Thomas, M., and Younkin, R. L., "Rocket Plume Optical Signature," CR-5-244, Oct. 1972, McDonnell Douglas Astronautics Co.—West, Huntington Beach, Calif.

[7] Plass, G. N., "Mie Scattering and Absorption Cross Sections for Aluminum Oxide and Magnesium," *Applied Optics*, Vol. 3, No. 7, July 1964, pp. 867–872.

[8] Bauer, E. and Carlson, D. J., "Mie Scattering Calculations for Micron Size Alumina and Magnesia Spheres," *Journal of Quantitative Spectroscopy and Radiative Transfer*, Vol. 4, No. 3, May–June 1964, pp. 363–374.

[9] Stull, D. R. and Prophet, H., *JANAF Thermochemical Tables*, 2nd ed., NSRDS-NBS 37, June 1971, National Bureau of Standards, Washington, D.C.

[10] Streed, E. R., Cunnington, G. R., and Liu, C. K., "TARGET PHENOMENOLOGY: Task III: Experimental Determination of the Infrared Spectral Optical Properties of Bulk and Powered Aluminum Oxide (U)," LMSC Rept. D313095, TP-3550, (AFRPL Report 73-3), Dec. 1972, Lockheed Missiles and Space Co., Palo Alto, Calif.

Effective Moduli of Layered Composites

C. H. S. CHEN* AND F. TABADDOR†

The B. F. Goodrich Company, Akron, Ohio

Introduction

FORMULA for obtaining the effective moduli (or stiffnesses) of laminated composites are given in many references.[1–4] However, except for Ref. 4, they are all limited only to two-dimensional quantities (3 × 3 matrix) since the majority of composites are in the form of thin plates or shells. But when the layered composites are not in the form of thin plates or shells or when the plate or shell models are not suitable for the analysis, the layered composite has to be treated as anisotropic solid. In this case the properties associated with third direction can not be neglected. Therefore, it is necessary to generate a complete 6 × 6 matrix for elastic moduli which takes into account the properties in all three directions. The objective of this Note is to derive the complete moduli matrix for the class of anisotropic solid composed of layered media. In the present Note no limitation is imposed on the type of anisotropy each constituent layer can possess, whereas in Ref. 4 it is restricted to monoclinic anisotropy. Therefore the present treatment is more general than that of Ref. 4 and that it is carried out in more concise form, although the approaches of both are in principle the same. Explicit expressions are obtained for two-layered angle ply composite which is of most common interest to us. Although only the gross or approximate properties in the sense of composite theory are obtained here, they can be used in solving three-dimensional problems.

Received June 27, 1973; revision received November 20, 1973.

Index category: Structural Composite Materials.

* Senior Engineering Scientist. Member AIAA.

† Senior Engineering Scientist.

Basic Equations

Consider an infinitesimal element of composite media made of n layers of anisotropic material (Fig. 1). Each layer may have its planes of elastic symmetry in arbitrary orientation with respect to coordinate system. For the case of fiber reinforced material this implies that each layer may have arbitrary fiber orientation with respect to coordinate axes. Let us apply to this element a constant strain field $[\bar{e}_x]$ and constant stress field $[\bar{s}_z]$ where

$$[\bar{e}_x] = \begin{bmatrix} \bar{\varepsilon}_x \\ \bar{\varepsilon}_y \\ \bar{\gamma}_{xy} \end{bmatrix}, \qquad [\bar{s}_z] = \begin{bmatrix} \sigma_z \\ \tau_{yz} \\ \tau_{xz} \end{bmatrix} \tag{1}$$

It should be stated here that some of the notations used here may not have the same meanings as those commonly used in laminated plate theory and the readers should be cautious not to be confused with their definitions. The stress-strain relations for ith layer may then be written as

$$\begin{bmatrix} s_x{}^i \\ \bar{s}_z \end{bmatrix} = \begin{bmatrix} A_i & H_i \\ H_i{}^T & C_i \end{bmatrix} \begin{bmatrix} \bar{e}_x \\ e_z{}^i \end{bmatrix} \tag{2}$$

where

$$[s_x] = \begin{bmatrix} \sigma_x \\ \sigma_y \\ \tau_{xy} \end{bmatrix}, \qquad [e_z] = \begin{bmatrix} \varepsilon_z \\ \gamma_{yz} \\ \gamma_{xz} \end{bmatrix} \tag{3}$$

with superscript and subscript i denoting ith layer and superscript T denoting matrix transpose. A_i, H_i, C_i, and $H_i{}^T$ are submatrices in stiffness matrix. It should be noted here that A_i and C_i are both symmetric matrices.

Equations (2) give us

$$s_x{}^i = A_i \bar{e}_x + H_i e_z{}^i \tag{4}$$

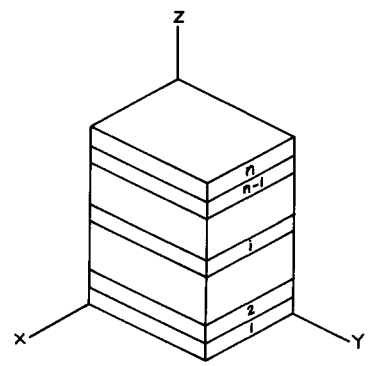

Fig. 1 Element of layered composite.